

Contactless dielectrophoresis: a new technique for cell manipulation

Hadi Shafiee · John L. Caldwell · Michael B. Sano · Rafael V. Davalos

Published online: 5 May 2009
© Springer Science + Business Media, LLC 2009

Abstract Dielectrophoresis (DEP) has become a promising technique to separate and identify cells and microparticles suspended in a medium based on their size or electrical properties. Presented herein is a new technique to provide the non-uniform electric field required for DEP that does not require electrodes to contact the sample fluid. In our method, electrodes are capacitively-coupled to a fluidic channel through dielectric barriers; the application of a high-frequency electric field to these electrodes then induces an electric field in the channel. This technique combines the cell manipulation abilities of traditional DEP with the ease of fabrication found in insulator-based technologies. A microfluidic device was fabricated based on this principle to determine the feasibility of cell

manipulations through contactless DEP (cDEP). We were able to demonstrate cell responses unique to the DEP effect in three separate cell lines. These results illustrate the potential for this technique to identify cells through their electrical properties without fear of contamination from electrodes.

Keywords BioMEMS · Biochip · Dielectrophoretic · Microfluidics · Sample handling · Electrorotation · Sample preparation

1 Introduction

Efficient biological particle separation and manipulation is a crucial issue in the development of integrated microfluidic systems. Current enrichment techniques for sample preparation include density gradient based centrifugation or membrane filtration (Giddings 1993), fluorescent and magnetic activated cell sorting (F/MACS) (Miltenyi et al. 1990), cell surface markers (Fu et al. 1999), and laser tweezers (Ashkin et al. 1987). Each of these techniques relies on different cell properties for separation and has intrinsic advantages and disadvantages. Typically, more sensitive techniques may require prior knowledge of cell-specific markers and antibodies to prepare target cells for analysis.

One alternative to these methods is dielectrophoresis (DEP) which is the motion of a particle due to its polarization in the presence of a non-uniform electric field (Pohl 1951, 1958). Currently, typical dielectrophoretic devices employ an array of thin-film interdigitated electrodes placed within the flow of a channel to generate a non-uniform electric field that interacts with particles near the surface of the electrode array (Yang et al. 1999). Such platforms have shown that DEP is an effective means to concentrate and differentiate cells rapidly and reversibly

Electronic supplementary material The online version of this article (doi:10.1007/s10544-009-9317-5) contains supplementary material, which is available to authorized users.

H. Shafiee · M. B. Sano · R. V. Davalos
Engineering Science and Mechanics Department, Virginia Tech,
Blacksburg, VA 24061, USA

J. L. Caldwell
Bradley Department of Electrical and Computer Engineering,
Virginia Tech,
Blacksburg, VA 24061, USA

R. V. Davalos
School of Biomedical Engineering & Sciences,
Virginia Tech—Wake Forest University,
Blacksburg, VA 24061, USA

H. Shafiee · J. L. Caldwell · M. B. Sano · R. V. Davalos (✉)
Cellular ElectroMechanical Systems (CEMS) Laboratory,
Institute for Critical Technology and Applied Science (ICTAS),
Virginia Tech,
Blacksburg, VA 24061, USA
e-mail: davalos@vt.edu

based on their size, shape, and intrinsic electrical properties such as conductivity and polarizability. These intrinsic properties arise due to the membrane compositional and electrostatic characteristics, internal cellular structure, and the type of nucleus (Gascoyne and Vykoukal 2004) associated with each cell type.

The application of DEP to separate target cells from a solution has been studied extensively in the last two decades. Examples of the successful use of DEP include the separation of human leukemia cells from red blood cells in an isotonic solution (Becker et al. 1994), entrapment of human breast cancer cells from blood (Gascoyne et al. 1997), and separation of U937 human monocytic from peripheral blood mononuclear cells (PBMC) (Huang et al. 2002). DEP has also been used to separate neuroblastoma cells from HTB glioma cells (Huang et al. 2002), isolate cervical carcinoma cells (Cheng et al. 1998), isolate K562 human CML cells (Altomare et al. 2003), separate live yeast cells from dead (Markx et al. 1994), and segregate different human tumor cells (Das et al. 2005). Unfortunately, the microelectrode-based devices used in these experiments are susceptible to electrode fouling and require complicated fabrication procedures (Hughes 2002; Steffen Hardt 2007).

Insulator-based dielectrophoresis (iDEP) is a practical method to obtain the selectivity of DEP while overcoming the robustness issues associated with traditional DEP platforms. iDEP relies on insulating obstacles rather than the geometry of its electrodes to produce spatial non-uniformities in the electric field. The patterned electrodes at the bottom of the channel employed by conventional DEP create an electric field gradient near their surface such that only cells in their vicinity are affected. One advantage of iDEP, is that the insulating structures typically traverse the entire depth of the channel and provide a non-uniform electric field over their entire depth, thus increasing the affected area. This advantage typically results in a higher throughput for the technique when compared to traditional DEP. The basic concept of the iDEP technique was first presented by Masuda et al. (Masuda et al. 1988). Others have previously demonstrated with glass insulating structures and AC electric fields that iDEP can separate DNA molecules, bacteria, and hematopoietic cells (Chou et al. 2002). It has been shown that polymer-based iDEP devices are effective for selective trapping of a range of biological particles in an aqueous sample (Davalos et al. 2008). iDEP technology has also shown the potential for water quality monitoring (Simmons et al. 2006), separating and concentrating prokaryotic cells and viruses (Lapizco-Encinas et al. 2005), concentration and separation of live and dead bacteria (Lapizco-Encinas et al. 2004), sample concentration followed by impedance detection (Sabounchi et al. 2008), and manipulation of protein particles (Lapizco-Encinas et al. 2008).

While many have had success designing and fabricating different DEP and iDEP microdevices to manipulate particles in biological fluids, there are some potential drawbacks of these techniques. The traditional DEP technique suffers from fouling, contamination, bubble formation near integrated electrodes, low throughput, and an expensive and complicated fabrication process (Hughes 2002; Steffen Hardt 2007). The insulating obstacles employed by iDEP are meant to address these shortcomings and are less susceptible to fouling than integrated electrodes (Cummings and Singh 2003). iDEP's fabrication process is also much less complicated; the insulating obstacles can be patterned while etching the microchannel in one step. This technique has the added benefit of making the process more economical in that mass fabrication can be facilitated through the use of injection molding. Unfortunately, one of the primary drawbacks of an iDEP system is the presence of a high electric field intensity within the highly conductive biological fluid inside the microchannel (Sabounchi et al. 2008; Steffen Hardt 2007). The relatively high electrical current flow in this situation causes joule heating and a dramatic temperature increase. The ideal technique would combine iDEP's simple fabrication process and resistance to fouling with DEP's reduced susceptibility to joule heating all-the-while preserving the cell manipulation abilities of both methods.

We have developed an alternative method to provide the spatially non-uniform electric field required for DEP in which electrodes are not in direct contact with the biological sample. The absence of contact between electrodes and the sample fluid inside the channel prevents bubble formation and mitigates fouling. It is also important to note that without direct contact between the electrodes and the sample fluid, any contaminating effects of this interaction can be avoided. In fact, the only material in contact with the sample fluid is the substrate material on which the device is patterned. In our method, an electric field is created in the microchannel using electrodes inserted in a highly conductive solution which is isolated from the main channel by thin insulating barriers. These insulating barriers exhibit a capacitive behavior and therefore an electric field can be produced in the main channel by applying an AC electric field across them. Furthermore, non-uniformity of the electric field distribution inside the main channel is provided by the geometry of insulating structures both outside and inside the channel.

In order to demonstrate this new method for cell separation and manipulation, we have designed and fabricated a microfluidic device to observe the DEP response of cells to a non-uniform electric field created without direct contact from electrodes. Modeling of the non-uniform electric field distribution in the device was accomplished through an equivalent electronic circuit and

finite element analysis of the microfluidic device. The effects of different parameters such as total applied voltage, applied frequency, and the electrical conductivity of the fluid inside and outside of the main channel on the resulting DEP response were simulated and then observed through experimentation. DEP responses for three different cell lines (THP-1, MCF-7, and MCF-10A) were observed primarily as a change in cell trajectory or velocity as it traveled through the device. Further evidence of this DEP response to the non-uniform electric field is provided by the electrorotation of cells, and their aggregation in “pearl chain” formations.

2 Theory

DEP is the motion of polarized particles in a non-uniform electric field toward the high (positive DEP) or low (negative DEP) electric field. The direction of the force depends on the particle’s polarizability compared with medium conductivity. The time-average dielectrophoretic force is described as (Pohl 1951, 1958):

$$F_{DEP} = 2\pi\epsilon_m r^3 \text{Re}\{K(\omega)\} \nabla(\mathbf{E}_{rms} \cdot \mathbf{E}_{rms}) \tag{1}$$

where ϵ_m is the permittivity of the suspending medium, r is the radius of the particle, and \mathbf{E}_{rms} is the root mean square electric field. $\text{Re}\{K(\omega)\}$ is the real part of the Clausius-Mossotti factor $K(\omega)$. The Clausius-Mossotti is given by:

$$K(\omega) = \frac{\epsilon_p^* - \epsilon_m^*}{\epsilon_p^* + 2\epsilon_m^*} \tag{2}$$

where ϵ_p^* and ϵ_m^* are the complex permittivities of the particle and the medium, respectively. Complex permittivity is defined as:

$$\epsilon^* = \epsilon + \frac{\sigma}{j\omega} \tag{3}$$

where ϵ and σ are the real permittivity and conductivity of the subject, $j = \sqrt{-1}$ and ω is the radial frequency.

Electrorotation is the rotation of polarized particles suspended in a liquid due to an induced torque in a rotating electric field (Arnold 1982). The maximum magnitude of the torque is given by:

$$\Gamma = -4\pi\epsilon_m r^3 \text{Im}\{K(\omega)\} (\mathbf{E}_{rms} \cdot \mathbf{E}_{rms}) \tag{4}$$

where $\text{Im}\{K(\omega)\}$ is the imaginary part of the Clausius-Mossotti factor $K(\omega)$.

Assuming the cells are spherical particles in the medium, the hydrodynamic frictional force, f_{Drag} , due to translation

and hydrodynamic frictional torque, R , due to rotation are given by:

$$f_{Drag} = 6\eta r \pi (\mathbf{u}_p - \mathbf{u}_f) \tag{5}$$

$$R = 8\eta \pi r^3 \Omega \tag{6}$$

where r is the particle radius, η is the medium viscosity, \mathbf{u}_p is the velocity of the particle, \mathbf{u}_f is the medium velocity, R is induced torque, and Ω is the electrorotation rate (rad.S⁻¹).

The magnitude of the steady state electrorotation rate, Ω , and translational velocity, \mathbf{u}_p , is determined by a balance between the induced torque and the hydrodynamic friction and between the induced dielectrophoretic force and Stoke’s drag force on a cell, respectively. In this preliminary study it should be noted that the effect of the acceleration term is considered to be negligible. The relationship is given by:

$$\Omega(\omega) = \frac{\epsilon_m}{2\eta} \text{Im}\left(\frac{\epsilon_p^* - \epsilon_m^*}{\epsilon_p^* + 2\epsilon_m^*}\right) \mathbf{E}_{rms} \cdot \mathbf{E}_{rms} \tag{7}$$

$$\mathbf{u}_p = \mathbf{u}_f - \mu_{DEP} \nabla(E \cdot E) \tag{8}$$

where μ_{DEP} is the dielectrophoretic mobility of the particle and is defined as:

$$\mu_{DEP} = \frac{\epsilon_m r^2}{3\eta} \text{Re}\left(\frac{\epsilon_p^* - \epsilon_m^*}{\epsilon_p^* + 2\epsilon_m^*}\right) \tag{9}$$

3 Methods

3.1 Microfabrication process

3.1.1 Deep reactive ion etching (DRIE)

A silicon master stamp was fabricated on a <100> silicon substrate. AZ 9260 (AZ Electronic Materials) photoresist was spun onto a clean silicon wafer and softbaked at 114°C for 45 s (Fig. 1(a)). The wafer was then exposed to UV light for 45 s with an intensity of 12 W/m through a chrome-plated glass mask. The exposed photoresist was then removed using Potassium-based buffered developer AZ400K followed by another hard baking at 115°C for 45 s (Fig. 1(b)). Deep Reactive Ion Etching (DRIE) was used to etch the silicon master stamp to depths ranging from 50-100 microns (Fig. 1(c)). The silicon master stamp was then cleaned with acetone to remove any remaining photoresist (Fig. 1(d)). The scalloping effect, a typical effect of the

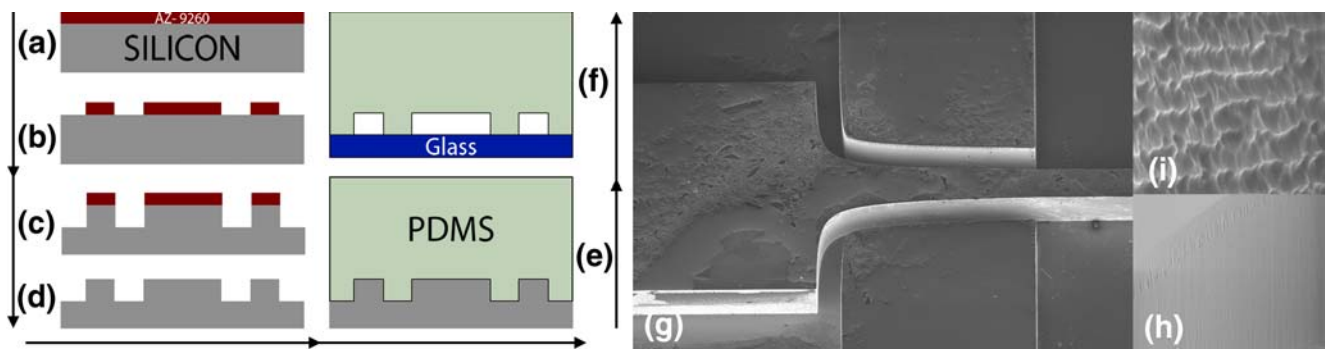


Fig. 1 (a–i) Schematic of the fabrication process used to create the microfluidic chambers and the SEM image of the scalloping effect on the silicon master. Steps (a) through (d) are followed only once to create a master stamp. Steps (e) and (f) are repeated to produce an indefinite number of experimental devices. (g) SEM image of the

silicon wafer mold at the intersection between the side and the main channel of the microfluidic device. (h) Surface roughness of the wafer after growing and removing the oxide layer. (i) Scalloping effect after DRIE

DRIE etching method, creates a surface roughness which is detrimental to the stamping process. In order to reduce the surface roughness, silicon oxide was grown on the silicon master using thermal oxidation and then was removed (Fig. 1(g–i)).

3.1.2 PDMS

The liquid phase PDMS was made by mixing the PDMS monomers and the curing agent in a 10:1 ratio (Sylgard 184, Dow Corning, USA). Bubbles in the liquid PDMS were removed by exposing the mixture to vacuum for an hour. An enclosure was created around the wafer using aluminum foil in order to contain the PDMS on the wafer as well as to ensure the proper depth for the PDMS portion of the device. The clean PDMS liquid was then poured onto

the silicon master and 15 min was allowed for degassing. The PDMS was then cured for 45 min at 100°C (Fig. 1(e)) and then removed from the mold. Finally, fluidic connections to the channels were punched with 15 gauge blunt needles (Howard Electronic Instruments, USA).

3.1.3 Bonding

Microscope glass slides (3" × 2" × 1.2 mm, Fisher Scientific, USA) were cleaned with soap and water, rinsed with distilled water and isopropyl alcohol, then dried with a nitrogen gun. The PDMS replica was bonded with the clean glass slides after treating with oxygen plasma for 40 s at 50 W RF power (Fig. 1(f)). A schematic with dimensions and equivalent circuit model of our device is presented in (Fig. 2(a)). The channel depth in this device is 100 μm and

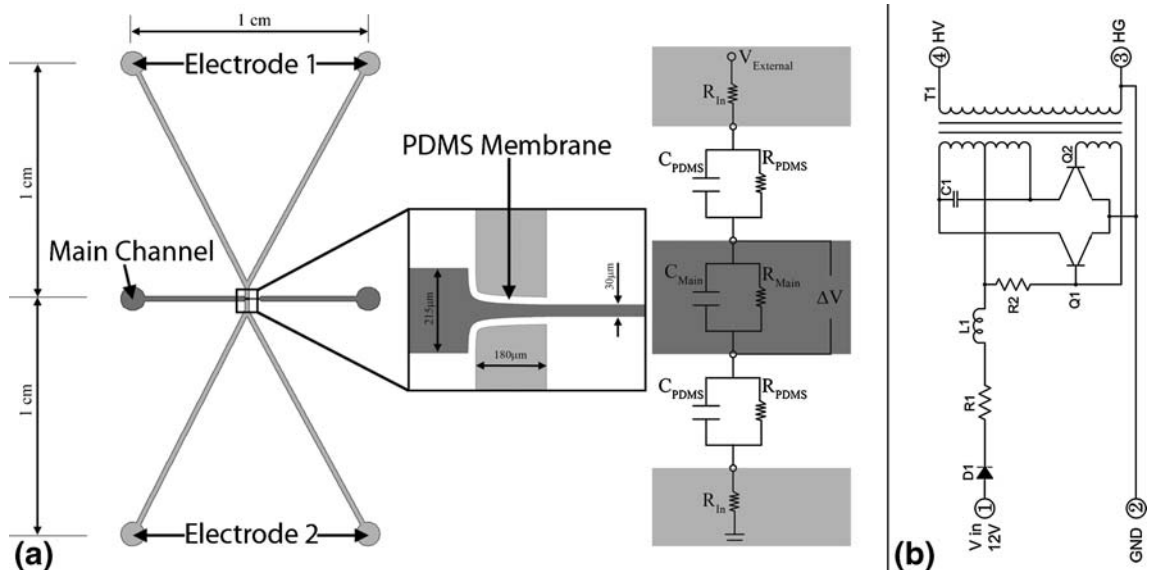


Fig. 2 (a) Schematic of the microfluidic device and the equivalent circuit model. (b) Schematic of the two transistor inverter circuit provided by JKL Components Corp

Table 1 Electrical properties of the materials and fluids

Electrical Properties Materials	Electrical Conductivity (S/m)	Relative Electrical Permittivity
PDMS	0.83 e-12	2.65
PBS	1.4	80
DEP Buffer	0.01	80

the thickness of the PDMS barrier between the side channels and the main channel is 20 μm .

3.1.4 Experimental setup

Pipette tips, inserted in the punched holes in the PDMS portion of the device, were used as reservoirs for fluidic connections to the channels. Pressure driven flow (10 to 15 $\mu\text{l/hr}$) was provided by an imbalance in the amount of the sample in these reservoirs of the main channel. An inverted light microscope (Leica DMI 6000B, Leica Microsystems, Bannockburn, IL) equipped with a digital camera (Hamamatsu EM-CCD C9100, Hamamatsu Photonics K.K. Shizuoka Pref., 430-8587, Japan) was used to monitor cells in the main channel. Microfluidic devices were placed in a vacuum jar for at least half an hour before running the experiments to reduce priming issues and then the side and main microchannels were filled with PBS and DEP buffer, respectively.

3.1.5 Cells and buffer

The THP-1 human Leukemia monocytes, MCF-7 breast cancer cells, and MCF-10A breast cells were washed twice and resuspended in our prepared DEP buffer (8.5% sucrose [wt/vol], 0.3% glucose [wt/vol], and 0.725% [vol/vol] RPMI) (Flanagan et al. 2008). The electrical conductivity of the buffer was measured with a Mettler Toledo SevenGo Pro conductivity meter (Mettler-Toledo, Inc., Columbus, OH) to ensure that its conductivity was 100 $\mu\text{S/cm}$. These cells were observed to be spherical when in suspension. The measured diameters of the cells with the corresponding standard deviations ($n=30$) are given in Table 2.

3.1.6 Electronics

A commercially available two-transistor inverter circuit (BXA-12576, JKL Components Corp., USA) was modified to provide a high-frequency and high-voltage AC signal for the device (Fig. 2(b)). The circuit relies on the oscillation created by the two-transistors and passive components to create an AC voltage on the primary side of a transformer. This voltage is then stepped-up by the transformer to give a high-output voltage on the secondary side to which the microfluidic device was connected.

The resonant frequency at which the circuit operates is highly dependent on the load impedance connected to the secondary side of the transformer. Two high-voltage power supplies were fabricated with resonant frequencies of 85 kHz and 125 kHz. A DC input voltage was provided by a programmable DC power supply (PSP-405, Instek America Corp., USA) which allowed adjustment of the output voltage by varying the input voltage. This technique allowed the output voltage of the power supplies to be varied from approximately 100 Vrms to 500 Vrms. A three-resistor voltage divider network, with a total impedance of one megaohm, was added to the output of the inverter circuit in order to provide a scaled (100:1) output voltage to an oscilloscope (TDS-1002B, Tektronix, USA) which facilitated monitoring the frequency and magnitude of the signal applied to the microfluidic device. All circuitry was housed in a plastic enclosure with proper high-voltage warnings on its exterior and connections were made to the microfluidic device using high-voltage test leads.

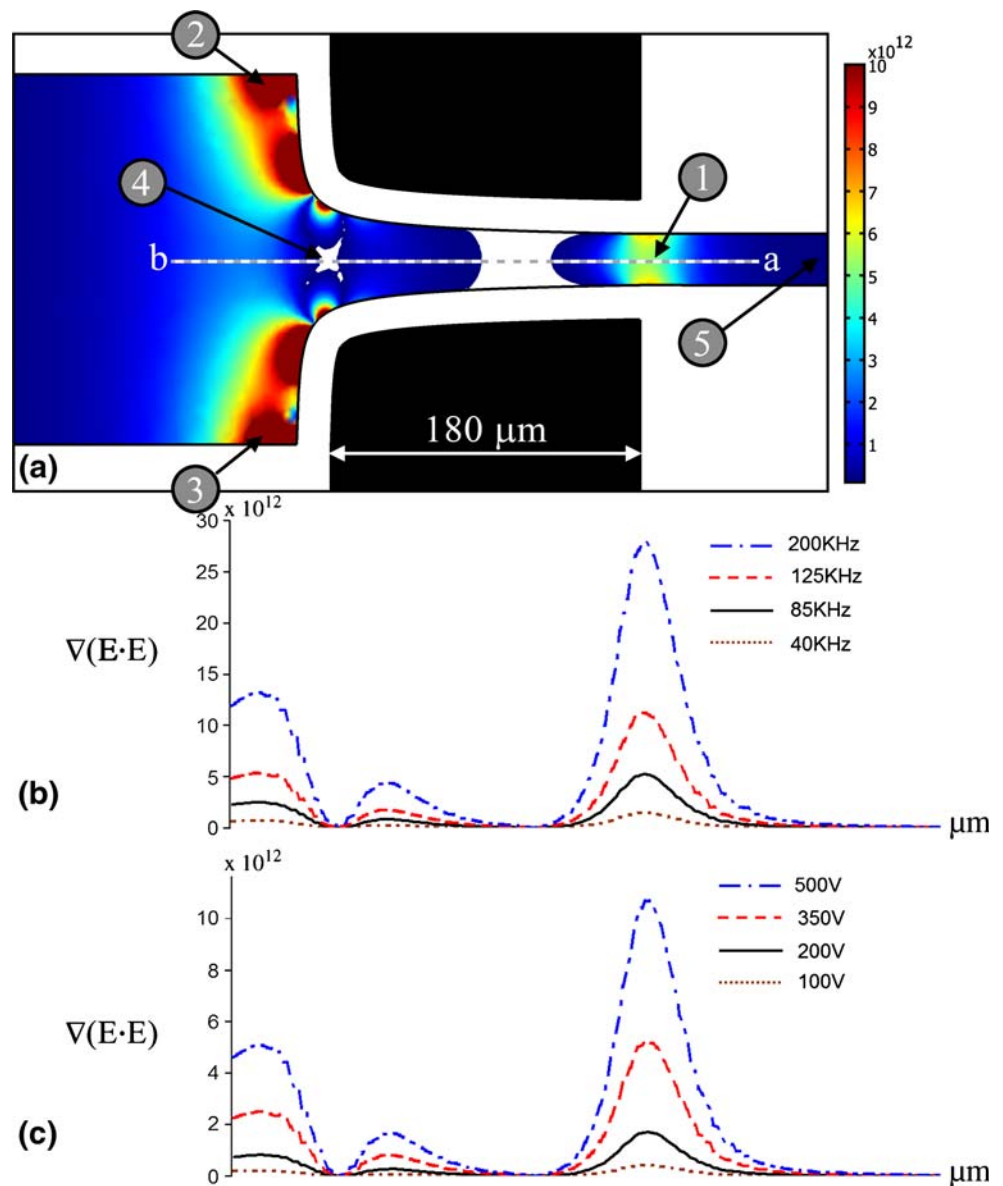
3.1.7 Translational and rotational velocity measurement

The average velocity of the THP-1, MCF-7 and MCF-10A cells in our microfluidic device was measured along the centerline a-b in Fig. 3 from point 1 to point 4. Time-lapse videos were recorded of the cells motion before and after applying an AC electric field through the platinum electrodes inserted in the side channels. These recorded videos then were converted to JPEG files using the Leica software, (Leica DMI 6000B, LAS AF 1.6.3 Leica Micro-

Table 2 The measured average velocity from point 1 to point 4 (Fig. 3) of five different cells before and after applying the electric field at the zone of trapping

Cell Velocity Cell line	Diameter (μm)	U_{on} ($\mu\text{m/s}$)	U_{off} ($\mu\text{m/s}$)	$U_{\text{off}} - U_{\text{on}}$ ($\mu\text{m/s}$)	$U_{\text{on}}/U_{\text{off}}$	Ω (rad/s)
THP-1	15.4 \pm 2	240 \pm 13	392 \pm 21	152 \pm 19	0.61 \pm 0.08	8.1 \pm 0.66
MCF-7	18.5 \pm 2.5	387 \pm 7	476 \pm 17	89 \pm 17	0.81 \pm 0.04	19.4 \pm 2.9
MCF-10A	18.2 \pm 2.1	310 \pm 17	313 \pm 16	3 \pm 24	0.99 \pm 0.076	N.A.

Fig. 3 Numerical results of the electric field gradient within the sample channel (a) Surface plot of the gradient of the field ($\text{kg}^2\text{mC}^{-2}\text{S}^{-4}$) within the main microchannel (b) Line plot of the gradient ($\text{kg}^2\text{mC}^{-2}\text{S}^{-4}$) along the line a-b (mm) for four different frequencies (40 kHz, 85 kHz, 125 kHz, and 200 kHz) at 250 Vrms (c) The line plot of the gradient of the electric field along the line a-b for four different applied voltages (100 V, 200 V, 350 V, and 500 V) at 85 kHz



systems, Bannockburn, IL), in order to measure the traveling time of the target cells for a known specific distance in the main channel. These measurements were performed before and after inducing the electric field in the main microfluidic channel.

3.2 Numerical modeling

The microfluidic device was modeled numerically in Comsol multi-physics 3.4 using the AC/DC module (Comsol Inc., Burlington, MA, USA). Because DEP

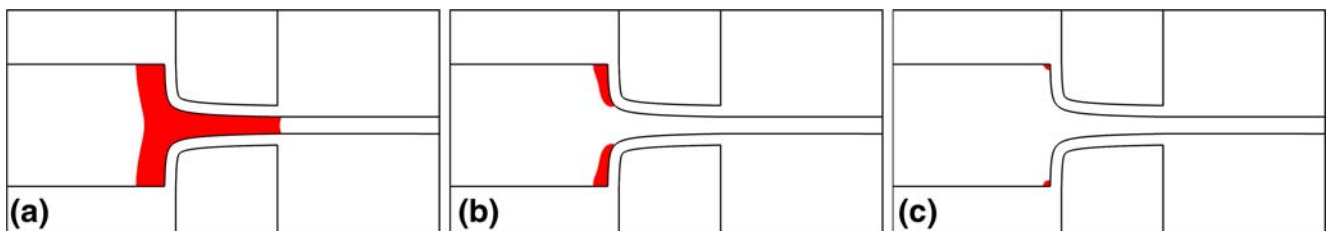
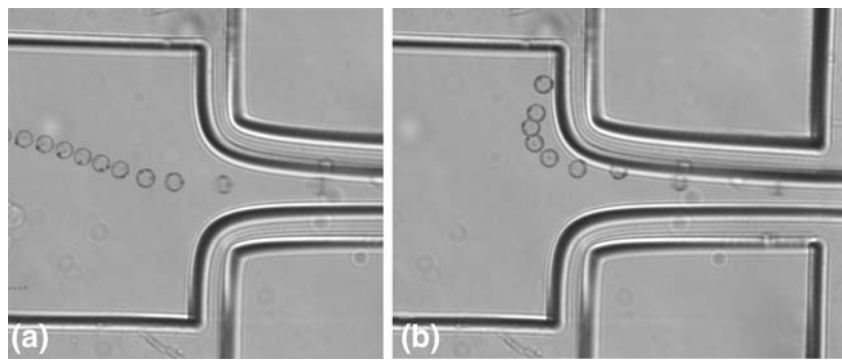


Fig. 4 Electric field surface plot for an applied AC field at 85 kHz and 250 Vrms. Areas with the induced electric field intensity higher than (a) 0.1 kV/cm, (b) 0.15 kV/cm, (c) 0.2 kV/cm

Fig. 5 Superimposed images showing the trajectory of one cell through the device. (a) The cell is moving from right to left under an applied pressure (b) with an applied voltage of 250 Vrms at 85 kHz. The superimposed images were approximately 250 ms apart



depends on the gradient of the electric field, $\nabla E = -\nabla(\nabla\phi)$ the first step in modeling was to determine the electric field distribution within a channel's geometry. This was done by solving for the potential distribution, ϕ , using the Laplace equation, $\nabla^2\phi = 0$. The boundary conditions used are prescribed uniform potentials at the inlet or outlet of the side channels.

The values for the electrical conductivity and permittivity of the PDMS, PBS, and DEP buffer that were used in this numerical modeling are given in Table 1. PBS and DEP buffer electrical properties are used for the side and main microfluidic channels, respectively.

The effect of the external voltage and the frequency on the gradient of the induced electric field has been studied. The gradient of the electric field along the center line of the main channel is investigated numerically for different applied voltages (100 V, 200 V, 350 V, and 500 V) at 85 kHz and for different frequencies (40 kHz, 85 kHz, 125 kHz, and 200 kHz) at 250 Vrms applied voltage. Based on our current available electronic circuit (250Vrms at 85 kHz), the electric field distribution and the gradient of the electric field was mapped in our microfluidic device.

4 Results and discussion

4.1 Numerical results

Figure 3 shows the surface and line plot of the gradient of the electric field inside the main microfluidic channel at the intersection between the main and the side channels. There is a high gradient of the electric field at the corners (points 2 and 3) as well as point 1, which can provide a strong DEP force. These results indicate that changes in the thickness of the PDMS barrier have a more significant effect on the gradient of the induced electric field inside the main channel than changes in the channel's geometry which is in agreement with our analytical results.

In (Fig. 3(b)) the gradient of the electric field along the line a-b is plotted for different applied frequencies (40 kHz, 85 kHz, 125 kHz, and 200 kHz) at 250 Vrms. The effect of the total

external voltage across the microfluidic device on the gradient of the electric field (along the line a-b) is also investigated in (Fig. 3(c)). DEP response of the system is plotted for four different voltages (100 V, 200 V, 350 V, and 500 V) at 85 kHz.

An increased gradient of the electric field can be obtained by increasing the applied frequency or increasing the total applied voltage although it should be noted that adjusting the frequency will also affect the Clausius-Mossotti factor of the microparticles and needs to be considered. Also the induced gradient of the electric field in the main microfluidic channel is on the order of 10^{12} ($\text{kg}^2\text{mC}^{-2}\text{S}^{-4}$) which is strong enough for particle manipulations.

Based on this numerical modeling, the voltage drop across the $20\mu\text{m}$ PDMS barrier was 250 V for an applied total voltage of 500 V across the microfluidic electrode channels. This voltage drop is lower than the 400 V break down voltage for a $20\mu\text{m}$ PDMS channel wall. Thus, the DEP force can be amplified by adjusting the input voltage with some tolerance.

4.1.1 Electric field surface plot

Figure 4(a-c) shows the induced electric field intensity distribution inside the main microfluidic channel filled with the DEP buffer with a conductivity of $100\mu\text{S}/\text{cm}$. The highest electric field is induced at the zone of intersection between the main and the side channels and between the PDMS barriers. Figure 4(c) also shows that with an applied AC electric field of 250 Vrms and 85 kHz the electric field does not significantly exceed 0.2 kV/cm in the main microfluidic channel.

4.2 Experimental results

4.2.1 Cell trapping-contactless DEP evidence

Figure 5 shows the experimental results we attained using MCF-7 breast cancer cells and THP-1 leukemia cells in our device. The behavior of cells traveling through the device under static conditions was observed to be significantly different than when an electric field was applied to the device. Three induced DEP responses were studied, rotation, velocity changes, and chaining.

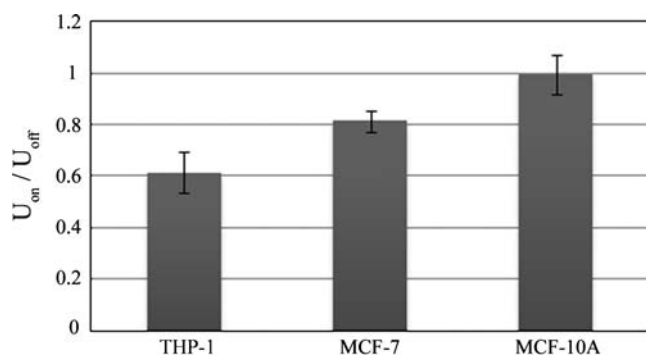
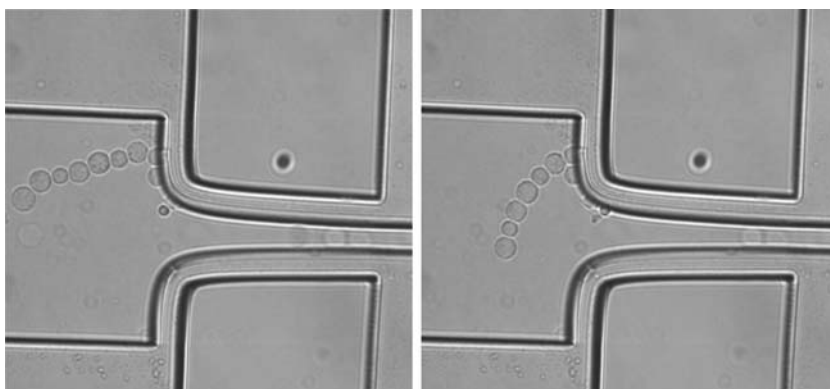


Fig. 6 The normalized velocity of THP-1, MCF-7, and MCF-10A cells. U_{on} is the velocity of the cells while applying e-field and U_{off} is the velocity of the cells while the power is off

Under a pressure driven flow, without an applied electric field, it was observed that THP-1 leukemia and MCF-7 breast cancer cells flow through the main microfluidic channel from right to left without any disruption or trapping. The cells were observed to be trapped, experiencing a positive DEP force, once an AC electric field at 85 kHz and 250 Vrms was applied. A representative video is given in the supplemental online data (supplemental online Video 1). Their velocity decreased at the intersection between the main and the side channels where the thin PDMS barriers are located. With the same electrical boundary conditions we did not observe any trapping or cell movement disruption for MCF-10A normal breast cells. These results indicate that the cells exhibited positive DEP at 85 kHz in our device. Furthermore, our results indicate that contact-less DEP may be an alternative method to DEP and iDEP to distinguish and separate cell types based on their Clausius-Mossotti factor.

Since the positive DEP force in the main microchannel depends on the electrical properties of the cells, different cell lines experience different forces at the same electrical boundary conditions (external voltage and frequency) in the same buffer. Cell bursting or lysis was not observed during cDEP trapping.

Fig. 7 Two, single-frame, showing several cells arranged in the “pearl-chain” phenomena often associated with DEP. These images show the grouping of cells into a chain configuration in areas of the main channel with a high gradient of the electric field. Images were captured with an applied field of 250 Vrms at 85 kHz



4.2.2 Translational velocity

The cells were observed to move faster along the centerline of the sample channel in (Fig. 3(a)) from point 5 to point 1 when the electric field was applied as compared to their velocity due to pressure driven flow. As shown in (Fig. 3), the magnitude of the DEP force is high at point 1. Because the DEP force is positive at 85 kHz, the cells are attracted to this point. Therefore, as the cells approach point 1 from the right, the positive DEP force is in the direction of the pressure driven flow, causing the cells to move faster down the channel. Conversely, the average velocity of the cells in the area between the thin PDMS barriers (from 1 to 4) decreases when the voltage is applied because the positive DEP force now acts in the opposite direction of the pressure driven flow.

Table 2 compares the average induced velocities of the cells with respect to their average velocities under pressure driven flow. The normalized velocity (U_{on} / U_{off}) for the three cell lines under the same electrical boundary conditions (250 Vrms at 85 kHz) are also reported in (Fig. 6). The results show that there is a statistically significant difference in the cells velocities when the field is applied. Furthermore, when the experiments are normalized for comparison, the results suggest that this technique can be used to differentiate cells based on their electrical properties.

The same experiments with the same buffers and electrical boundary conditions were performed on MCF-10A breast cells without noticeable trapping or disruption, which shows that the electrical properties of the normal breast cells are different compared to the MCF-7 breast cancer cells. It also shows the sensitivity of the cDEP technique to isolate cells with close electrical properties.

There was a great tendency for cells to move towards the corners in the main channel. This agrees with our numerical results, which show there is a high gradient of the induced electric field at the corners, which causes a strong positive DEP force and pulls cells towards these zones of the main microfluidic channel.

4.2.3 Rotational velocity

Cell rotation in the main channel at the zone of trapping and between the thin PDMS barriers was present with an applied electric field. The rotational velocity of the cell is a function of its electrical properties, the medium permittivity, the medium dynamic viscosity as well as the properties of the electric field. We measured the rotational velocity of the trapped THP-1, and MCF-7 cancer cells in different experiments at one spot of the main microfluidic channel. No cell rotation was observed without an applied electric field. The reported rotational velocities in Table 2 are the average rotational velocities of five different cells of each of the cancer lines. These results imply that the average rotational velocities of the THP-1 and MCF-7 cancer cell lines are significantly different. Cell rotation for the MCF-10A cells with the same electrical boundary conditions in the same buffer solution was not observed.

4.2.4 Pearl-chain

Cell aggregation and chain formation in DEP experiments with an AC field have been frequently observed and can be attributed to dipole-dipole interactions as well as local distortions of the electric field due to the cells' presence (Dussaud 2000; Pohl 1951, 1958; Wong 2004). Particles parallel to the electric field attract each other because of this dipole-dipole force, resulting in pearl-chaining of the trapped cells in the direction of the electric field in the microfluidic channel. The cell chain formation was observed for the MCF-7 and THP-1 cancer cell lines in our experiments with an applied AC electric field at 85 kHz and 250 Vrms (Fig. 7).

5 Conclusion

We have demonstrated a new technique for inducing electric fields in microfluidic channels in order to create a dielectrophoretic force. Our method relies on the application of a high-frequency AC electric signal to electrodes that are capacitively coupled to a microfluidic channel. In our device, the geometry of the electrode channels create the spatial non-uniformities in the electric field required for DEP. Three separate DEP responses were observed in our device, namely, translational velocity, rotational velocity, and chaining. In order to observe the devices effects in these three categories, three different cell lines were inserted into the devices and their individual responses recorded. Each cell line exhibited a response unique to its type due to the cell's specific electrical properties. This result highlights the ability of our technique to differentiate cells by their intrinsic electrical properties.

We believe this technique may help overcome many of the challenges faced with traditional DEP and iDEP.

Because the induced electric field is not as intense as comparable methods and is focused just at the trapping zones, we theorize the joule heating within the main microfluidic channel is negligible. This could mitigate the stability and robustness issues encountered with conventional iDEP (Sabounchi et al. 2008), due to the conductivity distribution's strong dependence on temperature. Furthermore, challenges associated with cell lysing due to high temperatures (Kang et al. 2008) or irreversible electroporation due to high field strengths (Davalos et al. 2005; Edd and Davalos 2007) are overcome with our new design approach under these conditions.

Acknowledgements This work was supported by the Institute for Critical Technology and Applied Science (ICTAS). Also the authors would like to acknowledge Dr. Eva M. Schmelz at the department of Human Nutrition, Foods, & Exercise and Phillip Andrew Zellner for their cooperation.

References

- L. Altomare, M. Borgatti, G. Medoro, N. Manaresi, M. Tartagni, R. Guerrieri, R. Gambari, *Biotechnol. Bioeng.* **82**, 474 (2003). doi:10.1002/bit.10590
- W. M. K. J. G. m. b. H. Arnold, Juelich (Germany, F.R.). *Inst. fuer Medizin*; Zimmermann, U. *Plant Physiol. Biochem.* **37**, 908 (1982)
- A. Ashkin, J.M. Dziedzic, T. Yamane, *Nature* **330**, 769 (1987). doi:10.1038/330769a0
- F.F. Becker, X.-B. Wang, Y. Huang, R. Pethig, J. Vykoukal, P.R.C. Gascoyne, *J. Phys. D. Appl. Phys. (Berl.)* **27**, 2659 (1994)
- J. Cheng, E.L. Sheldon, L. Wu, M.J. Heller, J.P. O'Connell, *Anal. Chem.* **70**, 2321 (1998). doi:10.1021/ac971274g
- C. Chou, J. Tegenfeldt, O. Bakajin, S. Chan, E. Cox, N. Damton, T. Duke, R. Austin, *Biophys. J.* **83**, 2170 (2002). doi:10.1016/S0006-3495(02)73977-5
- E.B. Cummings, A.K. Singh, *Anal. Chem.* **75**, 4724 (2003). doi:10.1021/ac0340612
- C.M. Das, F. Becker, S. Vernon, J. Noshari, C. Joyce, P.R. Gascoyne, *Anal. Chem.* **77**, 2708 (2005). doi:10.1021/ac048196z
- R.V. Davalos, G.J. McGraw, T.I. Wallow, A.M. Morales, K.L. Krafcik, Y. Fintschenko, E.B. Cummings, B.A. Simmons, *Anal. Bioanal. Chem.* **390**, 847 (2008). doi:10.1007/s00216-007-1426-5
- R.V. Davalos, L.M. Mir, B. Rubinsky, *Ann. Biomed. Eng.* **33**, 223 (2005). doi:10.1007/s10439-005-8981-8
- A.D. Dussaud, *J. Appl. Phys.* **88**, 5463 (2000). doi:10.1063/1.1315617
- J.F. Edd, R.V. Davalos, *Technol. Cancer Res. Treat.* **6**, 275 (2007)
- L.A. Flanagan, J. Lu, L. Wang, S.A. Marchenko, N.L. Jeon, A.P. Lee, E. S. Monuki, *Stem Cells* **26**, 656 (2008). doi:10.1634/stemcells.2007-0810
- A.Y. Fu, C. Spence, A. Scherer, F.H. Arnold, S.R. Quake, *Nat. Biotechnol.* **17**, 1109 (1999). doi:10.1038/15095
- P.R.C. Gascoyne, J.V. Vykoukal, *Proc. IEEE* **92**, 22 (2004). doi:10.1109/JPROC.2003.820535
- P.R.C. Gascoyne, X.-B. Wang, Y. Huang, F.F. Becker, *IEEE Trans. Ind. Appl.* **33**, 670 (1997). doi:10.1109/28.585856
- J.C. Giddings, *Science* **260**, 1456 (1993). doi:10.1126/science.8502990
- Y. Huang, S. Joo, M. Duhon, M. Heller, B. Wallace, X. Xu, *Anal. Chem.* **74**, 3362 (2002). doi:10.1021/ac011273v
- M.P. Hughes, *Electrophoresis* **23**, 2569 (2002). doi:10.1002/1522-2683(200208)23:16<2569::AID-ELPS2569>3.0.CO;2-M

- Y. Kang, D. Li, S.A. Kalams, J.E. Eid, *Biomed. Microdevices* **10**, 243 (2008). doi:[10.1007/s10544-007-9130-y](https://doi.org/10.1007/s10544-007-9130-y)
- B.H. Lapizco-Encinas, R.V. Davalos, B.A. Simmons, E.B. Cummings, Y. Fintschenko, *J. Microbiol. Methods* **62**, 317 (2005). doi:[10.1016/j.mimet.2005.04.027](https://doi.org/10.1016/j.mimet.2005.04.027)
- B.H. Lapizco-Encinas, S. Ozuna-Chacon, M. Rito-Palomares, *J. Chromatogr. A* **1206**, 45 (2008). doi:[10.1016/j.chroma.2008.05.077](https://doi.org/10.1016/j.chroma.2008.05.077)
- B.H. Lapizco-Encinas, B.A. Simmons, E.B. Cummings, Y. Fintschenko, *Anal. Chem.* **76**, 1571 (2004). doi:[10.1021/ac034804j](https://doi.org/10.1021/ac034804j)
- G.H. Markx, M.S. Talary, R. OPethig, *J. Biotechnol.* **32**, 29 (1994). doi:[10.1016/0168-1656\(94\)90117-1](https://doi.org/10.1016/0168-1656(94)90117-1)
- S. Masuda, T. Itagaki, M. Kosakada, *IEEE Trans. Ind. Appl.* **24**, 740 (1988). doi:[10.1109/28.6130](https://doi.org/10.1109/28.6130)
- S. Miltenyi, W. Muller, W. Weichel, A. Radbruch, *Cytometry* **11**, 231 (1990). doi:[10.1002/cyto.990110203](https://doi.org/10.1002/cyto.990110203)
- H.A. Pohl, *J. Appl. Phys.* **29** (1958)
- H.A. Pohl, *J. Appl. Phys.* **22**, 869 (1951)
- P. Sabounchi, D.E. Huber, A.E. Harris, B.A. Simmons, *MicroTAS Conference, San Diego* (2008).
- P. Sabounchi, A.M. Morales, P. Ponce, L.P. Lee, B.A. Simmons, R.V. Davalos, *Biomed Microdevices* **10**, 661 (2008). doi:[10.1007/s10544-008-9177-4](https://doi.org/10.1007/s10544-008-9177-4)
- B.A. Simmons, G.J. McGraw, R.V. Davalos, G.J. Fiechtner, Y. Fintschenko, E.B. Cummings, *MRS BULLETIN* **31**, 120 (2006)
- F. S. Steffen Hardt, *Microfluidic Technologies for Miniaturized Analysis Systems* (Springer, 2007). doi:[10.1007/978-0-387-68424-6](https://doi.org/10.1007/978-0-387-68424-6)
- P.K. Wong, *IEEE/ASME Transactions on Mechatronics* **9**, 366 (2004). doi:[10.1109/TMECH.2004.828659](https://doi.org/10.1109/TMECH.2004.828659)
- J. Yang, Y. Huang, X.B. Wang, F.F. Becker, P.R. Gascoyne, *Anal Chem* **71**, 911 (1999). doi:[10.1021/ac981250p](https://doi.org/10.1021/ac981250p)